

Scientific paper

Ternary Transition Metal Complexes with an Azo-Imine Ligand and 2,2'-Bipyridine: Characterization, Computational Calculations, and Acetylcholinesterase Inhibition Activities

Kerim Serbest,^{1,*} Turan Dural,¹ Demet Kızıl,³ Mustafa Emirik,¹
Ali Zengin² and Barbaros Dinçer¹

¹ Department of Chemistry, Recep Tayyip Erdogan University, 53100 Rize, Turkey

² Pazar Vocational School, Recep Tayyip Erdogan University, 53300 Pazar/Rize, Turkey

³ Central Research Laboratory, Bursa Technical University, 16310, Bursa, Turkey

* Corresponding author: E-mail: kerimserbest@yahoo.com
Tel.: +90 464 2234093

Received: 03-29-2022

Abstract

New mononuclear ternary transition metal complexes: $[M(\text{HL})(\text{bipy})_2]\text{ClO}_4$, (M: Mn(II) for **1**, Ni(II) for **2**), $[M(\text{HL})(\text{bipy})(\text{ClO}_4)]$, (M: Ni(II) for **3**, Cu(II) for **4**, Zn(II) for **5**) with M(II), 2-[(hydroxyimino)methyl]-4-[-phenyldiazenyl]phenol, H_2L , and 2,2'-bipyridine were synthesized, and their structures were investigated by using various analytical, spectroscopic techniques such as elemental analysis, FTIR, UV-Vis, NMR, MALDI-TOF mass spectrometry, thermal analysis. The theoretical studies were performed by DFT techniques by using B3LYP function with 6-311++G (d, p)/LanLD2Z basis set. The electronic transitions charters of the complexes were further analyzed by TD-DFT/CAM-B3LYP method. IR and thermal analysis data verify the proposed structures. The inhibition activities of the complexes against acetylcholinesterase (AChE) extracted from *Ricania simulans* adults and nymphs were examined and all the complexes were found to be active. Among the complexes studied, the highest inhibition activity was exhibited by complex **5** with the lowest IC_{50} value ($3.2 \pm 0.8 \mu\text{M}$) for AChE of adults and complex **3** with the lowest IC_{50} value ($4.6 \pm 0.8 \mu\text{M}$) for AChE of nymphs.

Keywords: Metal complex; TDDFT; AChE inhibitor, *R. simulans*.

1. Introduction

Coordination compounds with the azo-imine ligands have gained significant importance related to their applications in several high technology areas such as liquid crystalline displays (LCD), optical storage, laser and ink-jet printers as well as in leather, textile and plastic industries.^{1–3} They have attracted the attention of researchers because of their biological activities such as anti-microbial, antitumor, anticancer, anti-fungicidal.^{4–9} Numerous azo compounds are used in pharmaceuticals and cosmetics although some of them have been reported to be toxic.¹ Coordination compounds have also been investigated for the treatment of Alzheimer's disease (AD), Parkinson's dis-

ease, aging, and those showing inhibitor activity of AChE promise in the use of therapeutic applications.^{10–12} Some Co(II), Cu(II), Ni(II), Zn(II) complexes were reported as acetylcholinesterase inhibitors (AChEIs) and they also have the potential of use agricultural struggle because they are associated with excitation, tremors, and death in insects.^{10,13}

The agricultural areas located on the coastal part of the Eastern Black Sea Region have recently been exposed to the damage caused by a different type of insect known as *Ricania simulans* (Walker, 1851). It has been seen in this region for the past 9 years, despite the motherland which is known to be China.^{14,15} *R. simulans* is seen to be the type of pest where the population and the extended range of

which are on the increase with each passing day around this region.^{15,16} The Ricaniidae family, which belongs to the group of hemipteran insects, is represented by 40 stripes (types) and 400 species. Although the species of this family show general propagation in tropical regions, *Ricania* species can also be seen in Palearctic regions.^{15,17–19} It has a broad population in Japan, Southern China, Korea, Ukraine, Russia, and Georgia.^{15,20} Included in the quarantine list due to the harm it caused in Korea where *R. simulans* was brought from Southern Asia to Russia in the 1900s and to Georgia in the 1950s and also to the Eastern Black Sea Region of Turkey in 2006 along with the young trees with eggs and with bush saplings.¹⁵ Nymphs and adults of this pest that feed on vegetables, bushes, and trees without making a distinction of hosts rather harmful by absorbing the juice sap in the plant stems, leaves, and fruit. Tea gardens, which are among the most important product places of the coastline of the Eastern Black Sea Region, are under the threat of this pest, as well.¹⁵

Acetylcholinesterase (AChE, EC3.1.1.7) plays an important role in neurotransmission by hydrolyzing the neurotransmitter acetylcholine and is the target site of most insecticides. Vertebrates have both AChE and BuChE, whereas insects only have AChE.^{21,22} With the importance of AChE in neurotransmission and insect resistance, much attention has been paid to AChE studies from both mammals and insects. Most of these studies use non-purified AChE from homogenates of body parts or the whole body.²³ There is no study on the inhibition of acetylcholinesterase of *R. Simulans* with such complexes in the literature.

The density functional theory (DFT) is a useful tool for prediction of molecular structure, spectroscopic properties and chemical reactivity of molecular systems. Experimentally obtained spectroscopic results are supported by DFT-based theoretical calculations, which is a method frequently used recently. Since transition metal complexes

exhibit a wide variety of excited states, it remains difficult to accurately define the energy of excited states with the Time Dependent Density Functional Theory (TD-DFT). Because transition metal complexes exhibit a wide variety of excited states, it remains difficult to accurately describe the energy of excited states with the Time Dependent Density Functional Theory (TD-DFT). Common global descriptors of chemical reactivity of biologically active derivatives can be discussed using DFT methods.^{24–26}

The study presents the synthesis, characterization, DFT calculation for the assignment of experimental IR and UV–Vis spectra and acetylcholinesterase inhibition effects of mononuclear ternary transition metal complexes (1–5) derived from azo-imine ligand 2-[(hydroxyimino)methyl]-4-[-phenyldiazenyl]phenol, H₂L and 2,2'-bipyridine (bipy) as co-ligand (Figure 1) on AChEs of adults and nymphs of *Ricania simulans*. Because cell extract provides the closest composition to the cell medium, *R. simulans* extracts were used in the inhibition studies. This study is expected to be a starting point and of great importance in the exploration of metal-based insecticide.

2. Results and Discussion

2.1. NMR Spectra

Zn(II) complex, 5 has no solubility in common organic solvents, low solubility just in DMSO, and so the proton NMR spectra were taken with difficulty (Figure 2). The proton NMR spectral data of the Zn(II) complex given in the experimental section was compared with the ligands, and the data clearly proved the formation of mixed ligand Zn(II) complex. Phenolic and oxime hydroxyl group protons in the ligand were observed as a singlets at 10.98 and 11.60 ppm, respectively. The oxime hydroxyl proton signal was very broadened and shifted to 11.15 ppm, while the phenolic hydroxyl proton signal disappeared. The singlet of

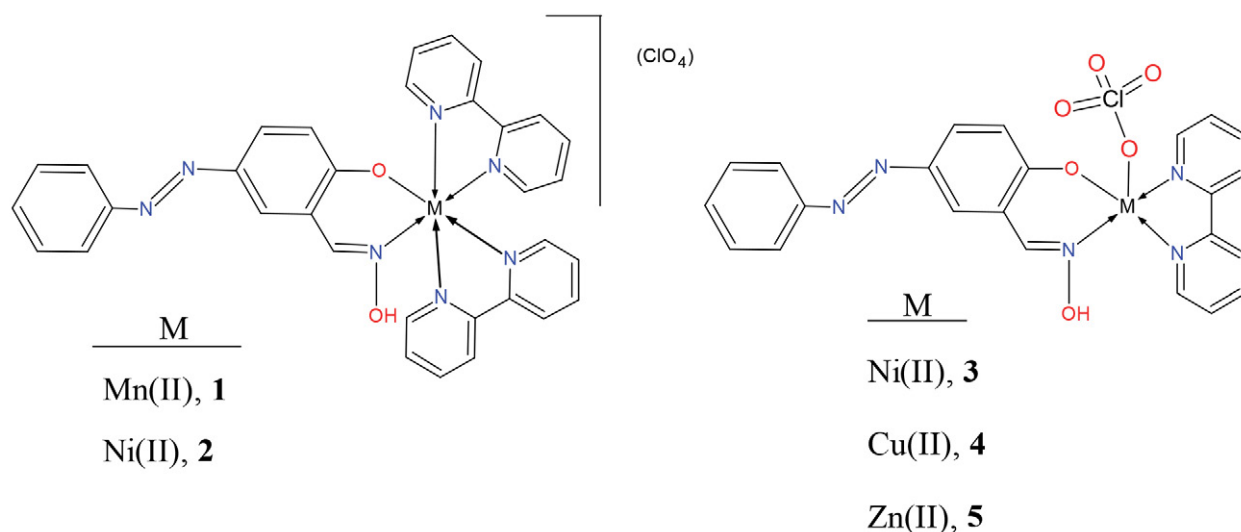


Figure 1: The proposed structures of the complexes (1–5) in the solid-state.

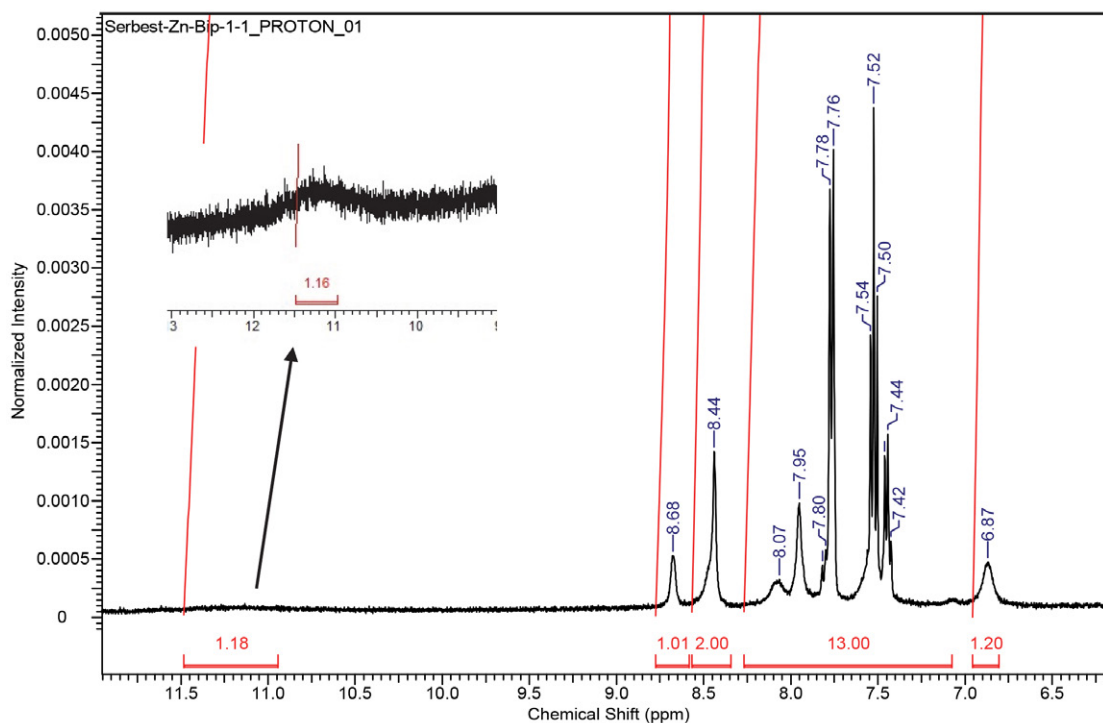


Figure 2: ^1H NMR spectra of Zn(II) complex, 5 in DMSO-d_6 .

imine proton was also slightly shifted to 8.44 ppm. The absence of phenolic OH proton and the low-field shift of the imine proton signal shows that the coordination of primary azo-oxime type ligand to Zn(II) ion is through the nitrogen of imine and phenolic oxygen atoms. The integrated intensities of the aromatic protons were also confirmed that Zn(II) complex contains a bipyridine molecule as co-ligand.

2. 2. Theoretical Calculations

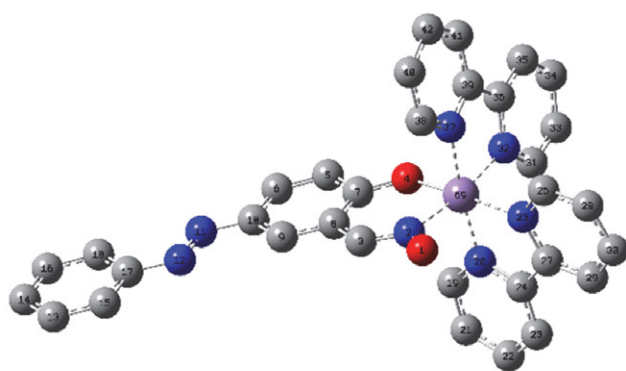
2. 2. 1. Molecular Structures

Geometry optimizations of the ligand and its corresponding complexes were performed using the Gaussian 09 program in the gas phase. The optimized geometry with

numbering and some of the optimized bond lengths, overlap populations, and bond orders around the metal center obtained from DFT calculations were given in Fig. 3–8.

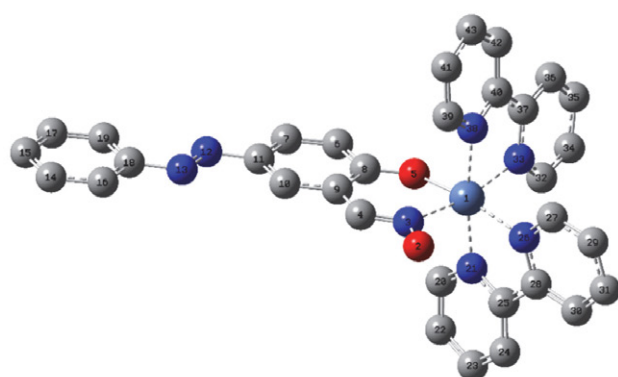
Complexes 1, 2, form six-coordinated octahedral while complexes 3, 4, and 5 have five-coordinated distorted square-pyramidal structures.

Addison, Reedijk and coworkers have proposed a geometry index for 5-coordinate transition metal complexes that can simply be calculated by taking the two largest angles around the metal center (Equation 1). The 5-coordinate index, $\tau_5 = 1$ is for a perfect trigonal bipyramidal structure and $\tau_5 = 0$ for a perfect square pyramidal structure.²⁷ The 5-coordinate index values of complexes 3, 4 and 5 were found as 0.46, 0.34 and 0.17, respectively. These complexes



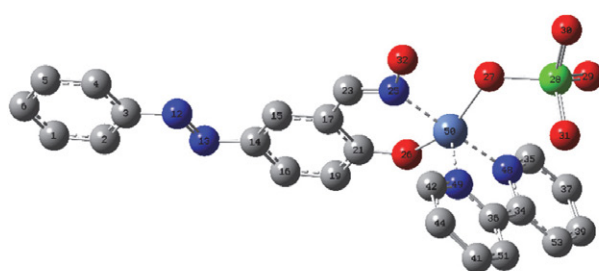
| Bond | L | OP | BO |
|----------|------|------|------|
| Mn69-N2 | 2.00 | 0.11 | 0.35 |
| Mn69-O4 | 1.94 | 0.23 | 0.60 |
| Mn69-N20 | 2.03 | 0.09 | 0.33 |
| Mn69-N25 | 2.05 | 0.08 | 0.31 |
| Mn69-N32 | 2.03 | 0.07 | 0.33 |
| Mn69-N37 | 2.04 | 0.08 | 0.33 |

Figure 3: Optimized molecular structure of complex 1 and selected bond length in Å (L), overlap population (OP) and bond order (BO).



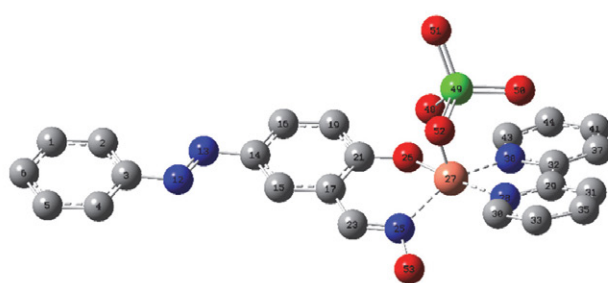
| Bond | L | OP | BO |
|---------|------|------|------|
| Ni1-N3 | 2.08 | 0.18 | 0.45 |
| Ni1-O5 | 2.01 | 0.24 | 0.59 |
| Ni1-N21 | 2.12 | 0.14 | 0.41 |
| Ni1-N26 | 2.18 | 0.12 | 0.37 |
| Ni1-N33 | 2.12 | 0.12 | 0.38 |
| Ni1-N38 | 2.12 | 0.13 | 0.40 |

Figure 4: Optimized molecular structure of complex 2 and selected bond length in Å (L), overlap population (OP) and bond order (BO).



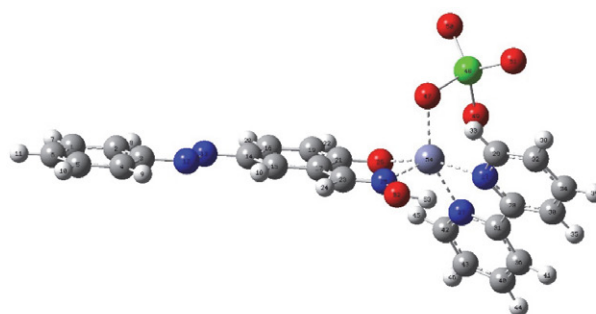
| Bond | L | OP | BO |
|----------|------|------|------|
| Ni50-N25 | 2.02 | 0.17 | 0.43 |
| Ni50-O26 | 1.96 | 0.20 | 0.56 |
| Ni50-N48 | 2.05 | 0.12 | 0.40 |
| Ni50-N49 | 2.04 | 0.15 | 0.46 |
| Ni50-O27 | 2.00 | 0.12 | 0.43 |

Figure 5: Optimized molecular structure of the complex 3 and selected bond length in Å (L), overlap population (OP) and bond order (BO).



| Bond | L | OP | BO |
|----------|------|------|------|
| Cu27-N25 | 2.04 | 0.18 | 0.44 |
| Cu27-O26 | 1.94 | 0.19 | 0.55 |
| Cu27-N28 | 2.05 | 0.16 | 0.44 |
| Cu27-O48 | 2.17 | 0.12 | 0.32 |
| Cu27-N38 | 2.04 | 0.16 | 0.43 |

Figure 6: Optimized molecular structure of the complex 4 and selected bond length in Å (L), overlap population (OP) and bond order (BO).



| Bond | L | OP | BO |
|----------|------|------|------|
| Zn54-N25 | 2.16 | 0.15 | 0.31 |
| Zn54-O26 | 2.00 | 0.18 | 0.40 |
| Zn54-N27 | 2.28 | 0.09 | 0.23 |
| Zn54-N37 | 2.16 | 0.12 | 0.28 |
| Zn54-O47 | 2.23 | 0.13 | 0.28 |

Figure 7: Optimized molecular structure of the complex 5 and selected bond length in Å (L), overlap population (OP) and bond order (BO).

have highly distorted coordination geometries intermediate between square-pyramidal and trigonalbipyramidal.²⁸

$$\tau_5 = (\beta - \alpha)/60 \quad (1)$$

Table 1. The two greatest valence angles around metal center for the complexes 3, 4, and 5.

| | | | |
|-----------|--------------|--------|-----------------|
| Complex 3 | N48-Ni50-N25 | 177.27 | $\tau_5 = 0.46$ |
| | O26-Ni50-O27 | 149.46 | |
| Complex 4 | N28-Cu27-O26 | 171.13 | $\tau_5 = 0.34$ |
| | N25-Cu27-N38 | 150.87 | |
| Complex 5 | N27-Zn54-O26 | 164.13 | $\tau_5 = 0.17$ |
| | O47-Zn54-N37 | 153.83 | |

The frontier orbitals' shape and the values of energies and energy gap were shown in Table 2. The energies of FMOs are important in several pharmacological and chemical fields. The electron-donating ability of a molecule is related to E_{HOMO} . The electron-accepting character of a molecule can be measured via E_{LUMO} values. The greater the E_{HOMO} is, the greater the electron donor capability, and the smaller the E_{LUMO} is the smaller the resistance to accept electrons.

The conceptual density functional theory-based descriptors can be useful to estimate the biological properties. The computed quantum chemical reactivity descriptors were illustrated in Table 3. The reactivity descriptors

including dipole moment, highest occupied molecular orbital energy (E_{HOMO}), lowest unoccupied molecular orbital energy (E_{LUMO}), chemical potential (μ), electronegativity (χ), hardness (η), softness (S), ionization potential (I), electron affinity (A), Electro-donating power (ω^-), electro-accepting power (ω^+), and net electrophilicity ($\Delta\omega$) were calculated using the following equations (2–10).

$$\mu = -\chi = (E_{HOMO} + E_{LUMO})/2 \quad (2)$$

$$\eta = E_{HOMO} - E_{LUMO} \quad (3)$$

$$I = -E_{HOMO} \quad (4)$$

$$A = -E_{LUMO} \quad (5)$$

$$S = 1/2\eta \quad (6)$$

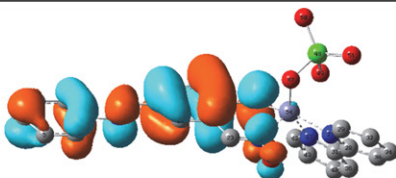
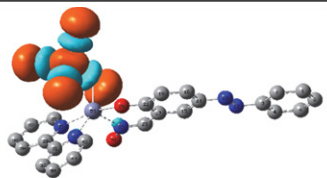
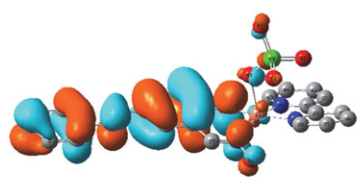
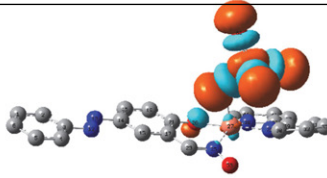
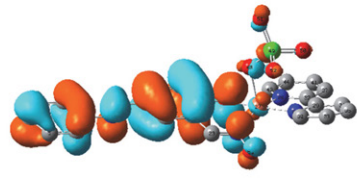
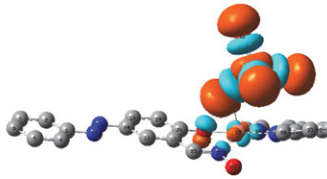
$$\omega = \mu^2/2\eta \quad (7)$$

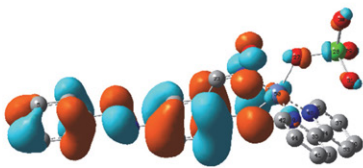
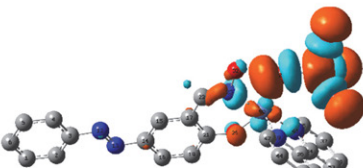
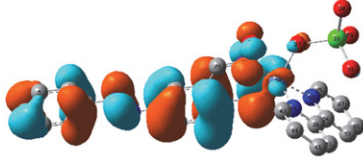
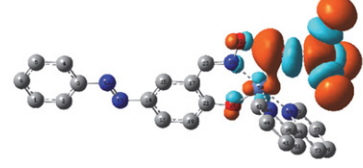
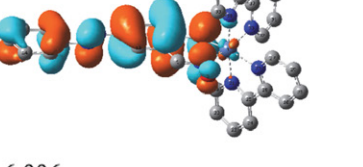
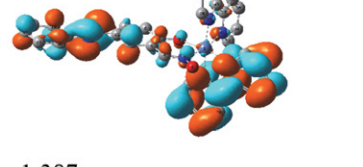
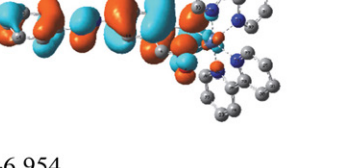
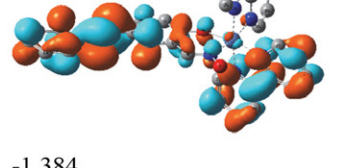
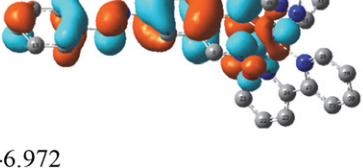
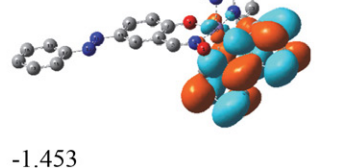
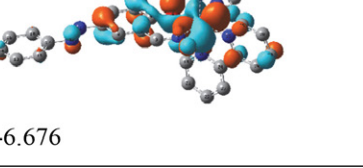
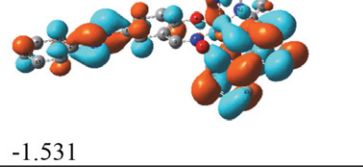
$$\omega^- = (3I + A)^2/16(I - A) \quad (8)$$

$$\omega^+ = (I + 3A)^2/16(I - A) \quad (9)$$

$$\Delta\omega = \omega^+ + \omega^- \quad (10)$$

Table 2. The frontier orbitals, energies, and energy gap of complexes in eV.

| | HOMO (eV) | GAP | LUMO (eV) |
|-----------|---|-------|--|
| 5 |  -7.059 | 3.456 |  -3.603 |
| 4 (Alpha) |  -6.067 | 1.755 |  -4.312 |
| 4 (Beta) |  -6.032 | 1.712 |  -4.320 |

| | HOMO (eV) | GAP | LUMO (eV) |
|-----------|---|-------|--|
| 3 (Alpha) |  -5.908 | 1.089 |  -4.819 |
| 3 (Beta) |  -5.933 | 1.198 |  -4.735 |
| 2 (Alpha) |  -6.996 | 5.609 |  -1.387 |
| 2 (Beta) |  -6.954 | 5.57 |  -1.384 |
| 1 (Alpha) |  -6.972 | 5.519 |  -1.453 |
| 1 (Beta) |  -6.676 | 5.145 |  -1.531 |

The chemical reactivity increases with increasing softness and according to the calculated softness values, complex 3 is more reactive than the other complexes. It is also expected that complex 2 has more activity due to biological activity is related to increased hardness. The hard-

ness value of complex 2 (5.57) is higher than that of other complexes and indicates that this complex is more stable. It is also known that stable molecules should have lower electrophilicity values. The net electrophilicity of complex 2 is lower than that of other complexes.^{29,30}

Table 3. The calculated quantum chemical descriptors (eV).

| Comp. | HOMO | LUMO | μ | χ | η | I | A | S | ω | ω^- | ω^+ | $\Delta\omega$ |
|-------|-------|-------|-------|--------|--------|------|------|------|----------|------------|------------|----------------|
| 1 | -6.68 | -1.53 | -4.10 | 4.10 | 5.15 | 6.68 | 1.53 | 0.10 | 1.64 | 5.65 | 1.54 | 7.19 |
| 2 | -6.95 | -1.38 | -4.17 | 4.17 | 5.57 | 6.95 | 1.38 | 0.09 | 1.56 | 5.55 | 1.38 | 6.94 |
| 3 | -5.91 | -4.82 | -5.36 | 5.36 | 1.09 | 5.91 | 4.82 | 0.46 | 13.21 | 29.17 | 23.80 | 52.97 |
| 4 | -6.03 | -4.32 | -5.18 | 5.18 | 1.71 | 6.03 | 4.32 | 0.29 | 7.82 | 18.34 | 13.17 | 31.51 |
| 5 | -7.06 | -3.60 | -5.33 | 5.33 | 3.46 | 7.06 | 3.60 | 0.14 | 4.11 | 11.10 | 5.77 | 16.88 |

2. 2. 2. Vibrational Assignments

All the IR spectra of the compounds were obtained using the FT-ATR technique in the region of 4000–650 cm^{-1} . The IR spectra of the mixed ligand complexes were compared with the starting ligands primary azo-oxime type ligand and bipyridine to determine the coordination sites that might be involved in chelation. All the vibrational signals of metal complexes (1-5) and primary ligand were calculated by using the DFT / B3LYP method to assign the experimental signals. Some selected vibrations and corresponding functional groups were summarized in Table 4.

In the IR spectrum of the azo-oxime ligand, signals of oxime protons (C=N–OH), –N=N– and C–O stretchings were observed at 3403, 1393, and 1265 cm^{-1} , respectively. The primary ligand has two OH groups which are oxime and phenolic OH. The primary ligand has two OH groups which are oxime and phenolic. But, the phenolic OH signal, which is expected to appear at a lower frequency than oxime OH, could not be observed due to possible intramolecular or intermolecular hydrogen bonding. In addition to the absence of phenolic OH stretching in the IR spectrum of the complexes, the broad bands observed at approximately 3440–3190 cm^{-1} were attributed to oxime OH stretchings. The intense C–O vibration of the primary ligand observed at 1265 cm^{-1} was shifted to the upper wave number in the complexes (1314–1287 cm^{-1}) and the intensity was also decreased compared to the free ligand. The medium intensity imine (C=N) vibration at 1621 cm^{-1} in the spectrum of the azo-oxime ligand shifted to the upper/lower wavenumber (1603–1645 cm^{-1}) and the intensity of this band increased/decreased usually in the complexes. These can be interpreted as the coordination of the metal ion to the primary ligand via the phenolic oxygen and nitrogen of imine.^{31,32}

Free 2,2'-bipyridine has a signal at 1577 cm^{-1} belonging to $\nu(\text{C}=\text{N})$ imine group. That the signal is observed at 1544 cm^{-1} for **5** and shifted to upper frequencies in the other complexes in the range of 1595–1606 cm^{-1} shows that the secondary bidentate ligand is coordinated to the metal center through nitrogen atoms of imine. Several bands belonging to the C=C vibrations were observed in the range of 1575–1437 cm^{-1} in the complexes. In addition, the characteristic out-of-plane C–H bending observed in 761–764 cm^{-1} was attributed to the bipyridine unit. Briefly, the obtained spectral data of the complexes confirm the

coordination of the primary ligand to the central metal ion via the imine and phenolic oxygen while 2,2'-bipyridine is coordinated through the nitrogen atoms.

IR spectra present evidence of the metal-perchlorate bond in solid-state. The perchlorate anion has a tetrahedral geometry, its point group is T_d , and it has four normal vibrational modes (ν_1 – ν_4) of the nine vibrational degrees of freedom of perchlorate, of which only two modes, the asymmetrical stretching (ν_3 , 1110 cm^{-1}) and asymmetrical bending (ν_4 , 626 cm^{-1}) are IR active.^{1,33} But, the ATR technique does not allow us to see the lower frequencies from 650 cm^{-1} . The diagnostic asymmetrical stretching band (ν_3) of ionic perchlorate is very broad and strong which is occasionally split. The minor shift and weak splitting of this band may be occurred because of the lattice effects as in **2**.³³ The Raman active symmetrical stretching band (ν_1) is theoretically forbidden in IR and observed as a weak band at 925–940 cm^{-1} . The diagnostic asymmetrical stretching band (ν_3) was observed at 1107 for **1** and 1082, 1071 cm^{-1} for **2** (See the supplementary file, Fig. S12, S13).³⁴

The asymmetrical stretching band (ν_3 , 1110 cm^{-1}) of the perchlorate group splits when a coordinate bond is formed between one of its oxygen atoms and central metal ion, so the symmetry of the perchlorate is lowered to C_{3v} , and number of vibrations increases. The bands are 1115, 1085, 1071 for **3**, 1158, 1113, 1071 for **4** and 1145, 1111, 1070 cm^{-1} for **5** (Fig. S14–16). The splittings confirm the monodentate coordination of the perchlorate ion in solid-state complexes (Table 3).³⁵ Based on IR data of **3**, perchlorate is coordinated monodentately. However, the conductivity data shows that complex **3**, which is compatible with the 1:1 electrolyte type, is solvolyzed in DMF.

2. 2. 3. UV-Vis Spectra

In order to evaluate experimental absorption bands, UV-Vis characteristics of the metal complexes were interpreted using the TDDFT/CPCM method in the implicit solvent of DMSO. The observed and predicted electronic spectra and their characters were summarized in Table 5. The calculated electronic transitions and FMO transitions that contribute to the formation of these bands are depicted in Table S1–S5. Experimentally observed bands were characterized according to contributions of molecular orbital

Table 4. Selected vibrational frequencies (observed and calculated, cm⁻¹) of synthesized compounds.

| Comp. | | $\nu(\text{C=N-OH})$ | $\nu(\text{C-H})$ | $\nu(\text{C=N})$ | Bipy, $\delta(\text{C-H})$ | $\nu(\text{C=C})$ | $\nu(\text{N=N})$ | $\nu(\text{C-O})$ | $\nu(\text{ClO}_4)$ |
|-----------------------|-------|----------------------|-------------------|-------------------|----------------------------|------------------------|-------------------|-------------------|--|
| H₂L | Exp. | 3403 | 3150–3000 | 1621 | – | 1569 | 1393 | 1265 | – |
| | Theo. | 3291(Ph), 3666 | 3074–2982 | 1654* | – | 1621–1590 | 1514 | 1289 | – |
| 1 | Exp. | – ^b | 3100–3050 | 1623, 1595* | 762 | 1519, 1468, 1439 | 1397 | 1300 | 1107(ν_3); 922(ν_1) |
| | Theo. | 3501 | 3113–3022 | 1611, 1593* | 755 | 1545–1610 | 1422 | 1299 | – |
| 2 | Exp. | 3416 ^a | 3150–3000 | 1644, 1602* | 763 | 1575, 1494, 1472, 1440 | 1409 | 1314 | 1082, 1071(ν_3); 945(ν_1) |
| | Theo. | 3503 | 3095–3002 | 1620, 1613* | 761 | 1458–1567 | 1387 | 1283 | – |
| 3 | Exp. | 3408 ^a | 3100–3000 | 1644, 1606* | 763 | 1548, 1476, 1440 | 1409 | 1310 | 1115, 1085, 1071(ν_1, ν_4); 933(ν_2) |
| | Theo. | 3225 | 3126–3034 | 1632, 1620* | 762 | 1507–1620 | 1412, 1420 | 1301 | – |
| 4 | Exp. | 3440 ^a | 3185–3050 | 1645, 1602* | 764 | 1541, 1476, 1437 | 1406 | 1313 | 1158, 1113, 1071(ν_1, ν_4); 924(ν_2) |
| | Theo. | 3505 | 3146–3040 | 1603, 1629* | 789 | 1508–1621 | 1420 | 1310 | – |
| 5 | Exp. | 3190 ^a | 3100–3000 | 1603, 1544 * | 761 | 1477, 1441 | 1405 | 1287 | 1145, 1111, 1070(ν_1, ν_4); 920(ν_2) |
| | Theo. | 3499 | 3093–2999 | 1612, 1594* | 761 | 1542–1610 | 1418 | 1326, 1339 | – |

(a: broad, b: not observed, Exp.: observed experimentally, Theo.: Theoretically calculated, *: Bipy $\nu(\text{C=N})$)

transition and location of FMO on molecules. Since the magnetic susceptibility measurements provide information about the strength of the ligand field of the complexes

and the number of unpaired electrons, these measurements were taken into account in the spin assignment of the complexes in the DFT calculations using spin-only formula.

Table 5. The electronic spectral data and calculated electronic transitions of complex 1-5 and their contributions.

| Comp. | $\lambda_{\text{exp.}}$ (nm) in solid | $\lambda_{\text{exp.}}$ (nm) in DMF | $\lambda_{\text{theo.}}$ (nm) | Osc. Strength | Major contributions | | |
|----------|---------------------------------------|-------------------------------------|--|---------------|--|----------------------|--|
| 1 | 237 | 291 | 251 | 0.07 | H-2(A)→L+4(A) (18%), HOMO(A)→L+4(A) (19%) | | |
| | | | 265 | 0.33 | H-8(A)→LUMO(A) (12%), HOMO(A)→L+5(A) (10%) | | |
| | | | 266 | 0.12 | H-5(A)→L+2(A) (12%) | | |
| | | | 269 | 0.13 | H-8(A)→LUMO(A) (14%), H-1(A)→L+4(A) (14%) | | |
| | | | 374 | 398 | 374 | 0.11 | H-1(A)→L+2(A) (18%) |
| | | | 375 | | 0.73 | HOMO(A)→L+1(A) (38%) | |
| | 374 | 398 | 406 | 0.13 | H-1(A)→LUMO(A) (21%), HOMO(A)→L+3(A) (18%) | | |
| | | | 461 | 0.02 | HOMO(B)→L+2(B) (23%) | | |
| | | | 501 | 0.02 | HOMO(B)→LUMO(B) (28%), HOMO(B)→L+2(B) (24%) | | |
| | | | 570 | 0.02 | HOMO(B)→L+2(B) (24%) | | |
| 2 | 246 | 290 | 212 | 0.15 | H-1(B)→L+2(B) (12%) | | |
| | | | 218 | 0.19 | H-7(B)→L+9(B) (32%) | | |
| | | | 238 | 0.22 | H-2(B)→L+3(B) (13%), H-3(A)→L+3(A) (11%) | | |
| | | | 251 | 0.12 | H-3(B)→LUMO(B) (17%) | | |
| | | | 264 | 0.59 | H-4(B)→L+2(B) (18%), H-5(A)→L+2(A) (15%) | | |
| | | | 312 | 433 | 266 | 0.23 | H-4(B)→L+2(B) (19%), H-8(A)→LUMO(A) (15%) |
| | 331 | 0.23 | HOMO(A)→L+3(A) (40%), HOMO(B)→L+3(B) (41%) | | | | |
| | 377 | 1.05 | HOMO(B)→LUMO(B) (35%), HOMO(A)→L+1(A) (24%) | | | | |
| | 436 | 0.03 | H-8(B)→L+8(B) (10%) | | | | |
| | 383 | 433 | 447 | 0.02 | H-9(B)→L+8(B) (27%) | | |

| | | | | | |
|-----|-----|-----|-----|------|--|
| 3 | 245 | 362 | 329 | 0.03 | H-21(A)→LUMO(A) (42%) |
| | 311 | | 344 | 0.02 | H-2(A)→L+3(A) (17%), H-4(B)→L+1(B) (15%) |
| | 379 | | 366 | 0.02 | H-16(B)→LUMO(B) (20%), H-1(B)→L+4(B) (13%) |
| | | | 368 | 0.07 | HOMO(B)→L+7(B) (28%), H-16(B)→LUMO(B) (15%) |
| | | | 378 | 0.02 | H-6(A)→L+1(A) (37%), HOMO(B)→L+6(B) (13%) |
| | | | 381 | 0.03 | HOMO(B)→L+6(B) (18%), HOMO(A)→L+5(A) (13%) |
| | | 429 | 418 | 0.37 | HOMO(B)→L+4(B) (20%), HOMO(A)→L+2(A) (17%) |
| | | | 421 | 0.22 | HOMO(B)→L+4(B) (15%) |
| | | | 480 | 0.16 | HOMO(B)→L+2(B) (25%), HOMO(B)→L+4(B) (11%) |
| | 4 | 253 | 290 | 311 | 0.02 |
| | | | 325 | 0.01 | H-5(A)→L+1(A) (17%) |
| 372 | | | 343 | 0.02 | H-2(A)→L+1(A) (21%) |
| | | | 346 | 0.01 | H-1(A)→L+3(A) (18%), H-2(A)→L+1(A) (14%) |
| | | 367 | 376 | 0.05 | HOMO(A)→L+4(A) (63%), HOMO(A)→L+5(A) (10%) |
| | | | 380 | 0.16 | HOMO(A)→L+4(A) (24%), HOMO(B)→L+6(B) (23%) |
| | | | 410 | 0.08 | HOMO(A)→L+3(A) (73%) |
| | | | 416 | 0.60 | HOMO(A)→L+2(A) (28%), HOMO(B)→L+3(B) (29%) |
| | | 459 | 421 | 0.04 | H-5(B)→L+1(B) (39%), H-4(B)→L+1(B) (15%) |
| | | | 462 | 0.05 | H-3(B)→LUMO(B) (12%), HOMO(B)→L+2(B) (43%) |
| | | | 468 | 0.04 | HOMO(A)→L+1(A) (23%), H-3(A)→LUMO(A) (13%) |
| | | | 478 | 0.01 | HOMO(B)→L+2(B) (39%) |
| | | | 522 | 0.01 | H-1(B)→L+1(B) (16%), HOMO(B)→L+1(B) (10%) |
| 5 | | 248 | | 234 | 0.20 |
| | | 288 | 236 | 0.17 | H-2→L+6 (21%), HOMO→L+7 (12%) |
| | | | 250 | 0.09 | H-3→L+3 (28%), H-10→LUMO (25%) |
| | 292 | | 265 | 0.28 | H-5→L+4 (43%), H-5→L+2 (11%) |
| | | | 267 | 0.10 | H-5→L+4 (14%), H-11→LUMO (10%) |
| | | 352 | 314 | 0.03 | H-6→L+1 (75%), HOMO→L+6 (10%) |
| | 367 | | 322 | 0.16 | HOMO→L+6 (68%), H-6→L+1 (13%) |
| | | | 368 | 1.09 | HOMO→L+3 (87%) |
| | | | 385 | 0.01 | H-2→LUMO (71%) |
| | | | 413 | 0.02 | H-18→LUMO (33%) |

The manganese(II) complex, **1** which has a distorted octahedral geometry shows three bands at 291, 398, and 461 nm in the electronic spectrum. Considering the os-

cillator powers, the first dense band consists of $\pi \rightarrow \pi^*$ and $d \rightarrow \pi^*$ transitions, with a predominance of $\pi \rightarrow \pi^*$ transitions. The second band observed at 398 nm is mainly com-

posed of $d \rightarrow n$ transitions, and attributed to metal-to-ligand charge transfer (MLCT) transition. According to the theoretical calculations, the third absorbance observed at 461 nm is attributed to $d \rightarrow \pi^*$ transitions. The bands observed experimentally at 461 nm originate mainly in the HOMO(B) \rightarrow LUMO(B)/L+2(B) transition and can be interpreted as intra-ligand charge transfer according to the orbital character. Magnetic moment values of Mn(II) complex (**1**) were measured as 5.80 BM on the Gouy balance. Magnetic moment values measured at room temperature are compatible with $S = 5/2$.

The nickel(II) complex, **2** which has a distorted octahedral geometry shows two bands, at 290 and 433 nm. The first intense band is formed by the contribution of $\pi \rightarrow \pi^*$, $n \rightarrow \pi^*$ and ligand-to-metal charge transfer (LMCT) transitions, with a predominance of $\pi \rightarrow \pi^*$ transitions. Considering the second broadband, the contribution of $\pi \rightarrow \pi^*$ transitions is dominant. LMCT and d-d transitions were also contributed to the formation of this band. The measured magnetic moments of the synthesized Ni(II) complex, **2** are 2.89 B.M.

The distorted squarepyramid nickel(II) complex, **3** shows two absorbance bands at 362 and 429 nm. Considering the oscillatory power of the observed transitions for both bands, the contribution of $\pi \rightarrow \pi^*$ transitions is predominant, with the contribution of $\pi \rightarrow \pi^*$, $n \rightarrow \pi^*$ and $d \rightarrow \pi^*$ (MLCT) transitions. It can be said that the contribution of $d \rightarrow \pi^*$ transitions is very small. The measured magnetic moments of the synthesized Ni(II) complex, **3** are 2.60 BM.

Three bands were observed in the electronic spectrum of the copper(II) complex, **4**, which has a distorted squarepyramidal geometry, at 290, 367, and 459 nm. The first dense band is attributed to $\pi \rightarrow \pi^*$ transitions, the second band is attributed to $\pi \rightarrow \pi^*$ and $n \rightarrow \pi^*$ transitions, and the third band is attributed to the weighted contribution of $\pi \rightarrow \pi^*$, $n \rightarrow \pi^*$ and ligand-to-metal charge transfer transitions (LMCTs). The magnetic moments of the Cu(II) complex were measured as 2.14 BM. This observed value is consistent with the spin value of the Cu(II) ion containing an unpaired electron.

The zinc(II) complex, **5**, which has a distorted squarepyramidal geometry, two bands were observed at 288 and 352 nm in the electronic spectrum of compound **5** and attributed to $\pi \rightarrow \pi^*$ and $n \rightarrow \pi^*$ transitions. The Zn(II) complex is diamagnetic because the zinc ion is in the d^{10} system.

2. 3. Thermal Stabilities

In order to determine the metal/ligand ratio and to get information about their thermal stabilities of the ternary transition metal complexes (**1-5**) from ambient temperature to 1000 °C in the O_2 atmosphere, their thermal decomposition processes were investigated by TG/DTG/DTA techniques. All the complexes studied are air-stable and have

very high thermal stability from thermal data in Table 6. The TG curves of the complexes were given in Figure 8 (see Supplementary, Fig. S1-S5 for the DTA_{max}). The metal oxide residues in thermograms of the complexes are compatible with the proposed structures and their stoichiometry.

From the TG curve of $[Mn(HL)(bipy)_2] ClO_4$, **1** has one step decomposition stage which was observed within the temperature range of 150–507 °C and the DTA curve shows three exothermic peaks at 173, 285 and 473 °C. All of the organic moiety was removed from the structure above 507 °C and the final residue was attributed to MnO , its percentage was 10.0% (calc. 10.0%).

In case of $[Ni(HL)(bipy)_2] ClO_4$, **2**, TG curve has three exothermic decomposition steps within the range of 25–629 °C. A rapid first step decomposition was observed at 245–360 °C (with exothermic DTA peaks at 285 and 358 °C) assigned to removal HL and a bipyridine with a mass loss of 56.0% (calc. 55.9%). The exothermic second step at 360–458 °C (with exothermic DTA peaks at 410 °C) is assigned to removal ClO_4-O with a mass loss of 11.6% (calc. 11.7%). The second bipyridine molecule was removed at 459–630 °C (with exothermic DTA peaks at 505 °C) with a mass loss of 22.8% (calc. 22.8%) in the third step and final residue was assigned to NiO with a mass of 8.6% (calc. 9.51%).

In case of $[Ni(HL)(bipy)(ClO_4)]$, **3**, TG curve has three step decomposition stages within the range of 25–700 °C. The endothermic dehydration of 0.5 mol adsorbed water with a mass loss of 1.6% (calc. 1.6%) was observed at 25–55 °C (DTA_{max} at 41.2 °C) in the first step. The exothermic second step at 154–299 °C (DTA_{max} at 291 and 305 °C) is assigned to remove a bipyridine molecule with a mass loss of 29.5 (27.7). The primary ligand, HL, and ClO_4-O was removed at 299–691 °C (DTA_{max} at 422 and 520 °C) with a mass loss of 57.6 (58.4) in the third step and final residue was assigned to NiO with a mass of 11.3% (calc. 13.5%).

In case of $[Cu(HL)(bipy)(ClO_4)]$, **4**, TG curve has three step decomposition stages within the range of 25–647 °C. The endothermic dehydration of 0.6 mol adsorbed water with a mass loss of 1.9% (calc. 1.9%) was observed at 25–56 °C (DTA_{max} at 47 °C) in the first step. The exothermic second step at 180–342 °C (DTA_{max} at 231 °C) is assigned to remove a bipyridine molecule with a mass loss of 27.3 (27.3). The primary ligand, HL and ClO_4-O was removed at 342–647 °C (DTA_{max} at 370, 383, and 448 °C) with a mass loss of 54.2 (56.8) in the third step, and the final residue was assigned to NiO with a mass of 16.6% (calc. 14.2%).

From the TG curve of $[Zn(HL)(bipy)]ClO_4$, **5** has one step decomposition stage which was observed within the temperature range of 131–599 °C and the DTA curve shows four exothermic peaks at 187, 301, 368, 456 °C. All of the organic moiety was removed from the structure above 599 °C and the final residue was assigned to ZnO, its percentage was 15.70% (calc. 14.5%).

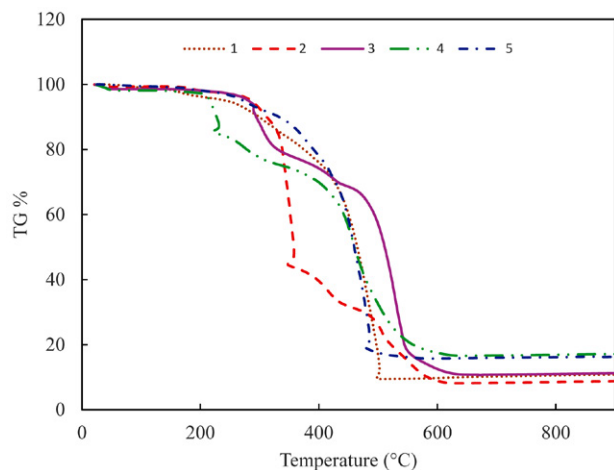


Figure 8: TG curves of the complexes (1-5).

Table 6. Thermal analysis data of the complexes.

| Comp. | Decom. Step(s) | Decom. Temp., °C | DTA _{max} , μV | Group lost, mass loss %, exp. (calc.) | Residue formula, Residue %, exp. (calc.) |
|-------|----------------|------------------|-----------------------------------|---|---|
| 1 | 1 | 150–507 | 173(+), 285(+), 473(+) | HL+2 bipy+ ClO ₄ -O 90.0 (90.0) | MnO, 10.0 (10.0) |
| | 1 | 245–360 | 285(+), 358(+) | HL+bipy 56.0 (55.9) | [Ni(bipy)] ClO ₄ , 43.1 (44.0) |
| 2 | 2 | 360–458 | 410(+) | ClO ₄ -O 11.6 (11.7) | [Ni(bipy)]O, 31.5 (32.6) |
| | 3 | 459–630 | 505(+) | Bipy 22.8 (22.8) | NiO, 8.6 (9.51) |
| | 1 | 25–55 | 41.2(-) | 0.5H ₂ O, 1.6, (1.6) | [Ni(HL)(bipy)(ClO ₄)], 98.4 (98.4) |
| 3 | 2 | 154–299 | 291(+), 305(+) | Bipy 29.5 (27.7) | [Ni(bipy)(ClO ₄)], 68.9 (98.4) |
| | 3 | 299–691 | 422(+), 520(+) | HL+ ClO ₄ -O 57.6 (58.4) | NiO, 11.3 (13.5) |
| | 1 | 25–56 | 47(-) | 0.6H ₂ O, 1.9, (1.9) | [Ni(HL)bipy] ClO ₄ , 98.1 (98.1) |
| 4 | 2 | 180–342 | 231(+) | Bipy 27.3 (27.3) | [Cu(HL)] ClO ₄ , 70.8 (70.8) |
| | 3 | 342–647 | 370(+), 383(+), 448(+) | HL+ ClO ₄ -O 54.2 (56.8) | CuO, 16.6 (14.2) |
| 5 | 1 | 131–599 | 187(+), 301(+), 368(+), 456(+) | HL+ bipy+ ClO ₄ -O 84.3 (85.5) | ZnO, 15.7 (14.5) |

2. 4. AChE Inhibition Studies

The synthesized complexes of Mn(II), Ni(II), Cu(II), and Zn(II) with mixed ligands exhibited inhibition activity against the AChEs of adults and nymphs of *R. simulans* (Table 7). On AChE of adults of *R. simulans*, the [Zn(HL)(bipy)(OCIO₃)], **5** (IC₅₀ = 3.2 ± 0.8 μM) showed an inhibition effect close to edrophonium chloride (IC₅₀ = 2.4 ± 0.3 μM) known as a competitive inhibitor of AChE. The [Mn(HL)(bipy)₂](ClO₄), **1** showed inhibition close to tacrine as an inhibitor of AChE, while

the other complexes showed better inhibition than tacrine.

Although the inhibitory effect of these complexes on the AChE of nymphs was not as much as edrophonium and tacrine, their effect on the AChE was quite high. Especially these were [Ni(HL)(bipy)(OCIO₃)] (**3**) (IC₅₀=4.6±0.8 μM), [Mn(HL)(bipy)₂](ClO₄) (**1**) (IC₅₀ = 5.6 ± 1.2 μM) and [Cu(HL)(bipy)(OCIO₃)] (**4**) (IC₅₀ = 6.4 ± 0.7 μM) complexes, and their inhibition concentrations were close to each other. It was observed that while [Zn(HL)(bipy)(OCIO₃)] (**5**) (IC₅₀ = 3.2 ± 0.8 μM) was more effective on adults, it had less effect on nymphs (IC₅₀ = 10.1 ± 2.4 μM). The inhibition effect of the [Ni(HL)(bipy)₂](ClO₄) (**2**) complex on both stages of *R. simulans* was observed to be the same at higher concentrations than the others. As a result of inhibition studies, it was determined that the [Zn(HL)(bipy)(OCIO₃)] complex was more effective

in the inhibition of AChE of the adults, and the [Ni(HL)(bipy)(OCIO₃)] complex was more effective in the inhibition of AChE of the nymphs.

Although the molecular mechanism is not fully known, it is suggested that metal complexes inhibit acetylcholinesterase by binding to both catalytic active site (CAS) and peripheral anionic site (PAS) in the active site of the enzyme.³⁶ Considering the structures of the complexes, complex **1, 2** may bind CAS site while complex **3-5** may bind PAS site of the enzyme. From the results it can be speculated that metal complexes with low coordination are

more likely to bind stronger than the others to the active site of the enzyme and a higher inhibitory effect may be expected.^{37,38}

While nymphs continue their lives in and around their hosts, they can spread to a wider area after they become adults. This implies that the sensory equipment, as well as the nervous system, must modify to accommodate the sensory requirements (such as host recognition, mate location, oviposition, aggregation, and defense) to the differences between nymphal and adult habitats. Therefore, adults are likely to have a more improved nervous system than nymphs.³⁹ In another literature, the differences in the activities of AChEs obtained from different stages of *Bactrocera dorsalis* (H.) were appraised from two perspectives. It was papered that one of them, some alterations to the protein structure occurred during the developmental stages to meet the continuously changing demands of the development of insects, the another factor, the differences in the expression level of genes encoding specific enzymes might be resulting in changes.⁴⁰ Because of such differences, it is normal for the AChEs from nymphs and adults of *R. simulans* to behave differently towards the inhibitors.

The inhibition effect of some copper complexes synthesized on acetylcholinesterase from *Electrophorus electricus* (eeAChE) was investigated and IC₅₀ values were determined between 5.45 ± 0.70 and 64.67 ± 2.20 μM.⁴¹

The effects of [Cu(naringin)₂], [Cu(naringenin)₂], Cu(hesperetin)₂, Cu(naringin)(2,2'-bipyridine), Cu(naringin)(phenanthroline), Cu(naringenin)(2,2'-bipyridine), Cu(hesperidin)(phenanthroline), Cu(hesperetin)(2,2'-bipyridine) and Cu(hesperetin)(phenanthroline) complexes on the activities of acetylcholinesterases obtained from human serum and electric eel were investigated. In this reported study, it was determined that the synthesized complexes have different effects on AChEs in different organisms. Also in this reported study, IC₅₀ values for huAChE were 1.73 ± 0.3, 0.66 ± 0.2, 0.33 ± 0.02, 0.012 ± 0.002, 0.87 ± 0.1, 0.25 ± 0.03, 0.32 ± 0.05, 0.33 ± 0.05, 0.36 ± 0.07 μM and IC₅₀ values for eeAChE were 0.16 ± 0.03, 1.41 ± 0.4, 2.55 ± 0.5, 0.17 ± 0.02, 1.4 ± 0.3, 0.46 ± 0.2, 1.77 ± 0.4, 0.94 ± 0.09, 0.33 ± 0.06 μM.¹³

Table 7. IC₅₀ values of acetylcholinesterase of *R. simulans* in the presence of the complexes (1-5).

| Complex | IC ₅₀ (μM) | IC ₅₀ (μM) |
|---|-----------------------|-----------------------|
| | For adults | For nymphs |
| [Mn(HL)(bipy) ₂] (ClO ₄), 1 | 22.0 ± 1.8 | 5.6 ± 1.2 |
| [Ni(HL)(bipy) ₂] (ClO ₄), 2 | 14.0 ± 1.2 | 16.5 ± 1.9 |
| [Ni(HL)(bipy)(OCIO ₃)], 3 | 16.0 ± 2.1 | 4.6 ± 0.8 |
| [Cu(HL)(bipy)(OCIO ₃)], 4 | 7.2 ± 1.4 | 6.4 ± 0.7 |
| [Zn(HL)(bipy)(OCIO ₃)], 5 | 3.2 ± 0.8 | 10.1 ± 2.4 |
| Edrophonium chloride | 2.4 ± 0.3 | 0.6 ± 0.09 |
| Tacrine | 18.0 ± 1.9 | 1.2 ± 0.4 |

3. Conclusions

The agricultural areas located on the coastal part of the Eastern Black Sea Region have recently been exposed to the damage caused by a different type of insect known as *Ricania simulans*. The acetylcholine esterase is the target site of most insecticides. So, mixed ligand metal complexes with azo-oxime ligand and 2,2'-bipyridine as co-ligand were prepared, theoretical calculations were performed to provide information about molecular geometry, electronic structure, molecular and spectroscopic properties. Additionally, their inhibitory activities against the AChEs of adults and nymphs of *R. simulans* in this study was reported. All the complexes were found to have inhibitor activities. Interestingly, complexes 4 and 5 showed better inhibitor activity than the other complexes tested and the most active of the complex has found to be complex, 5 with IC₅₀ value of 2.4±0.3 μM for adults, and complex 3 with the lowest IC₅₀ value (4.6±0.8 μM) exhibited the most inhibition activity for nymphs. Here, it has been shown that these complexes may be used as potential metal based insecticides against *R. simulans* which has posed a big challenge to the field of agriculture.

4. Experimental

4. 1. Materials and Methods

2,2'-Bipyridine (Bipy) and perchlorate salts of Mn(II), Ni(II), Cu(II), and Zn(II) were purchased from Merck. All chemical and solvents were analytical grade and used without any purification. 2-[(*E*)-(hydroxyimino) methyl]-4-[(*E*)-phenyldiazenyl]phenol, H₂L was prepared according to the reported literature.⁹

4. 2. Preparation of Crude Extract

About 5 g of adults or nymphs of *R. simulans* collected in July were homogenized in 20 mL phosphate buffer (pH 7.4, 0.05 M, containing 1 mM EDTA, 0.5% Triton X-100, 0.5 M NaCl) in the ice bath. The homogenates were centrifuged at 22,000xg for 30 min at 4 °C. After the supernatant was filtered via syringe filter units (pore size 0.45 μm). The supernatant was used as a crude extract.⁴²

4. 3. Measurements

Elemental analyses were measured with a LECO truspect analyzer and ¹H NMR spectra were measured with an Agilent Technologies 400/54 spectrometer at the Central Research Laboratory of Recep Tayyip Erdogan (RTE) University. MALDI-TOF mass spectra in a DHB matrix were recorded on a Bruker Microflex LT at the Gebze Institute of Technology for the complexes. IR spectra were recorded on a Perkin Elmer Spectrum 100 FT IR infrared spectrophotometer equipped with an ATR appa-

ratus. KBr is transparent in UV-Vis region, so solid-state electronic spectra for complexes were recorded on a SpectraMax M5 spectrophotometer in KBr discs. Magnetic susceptibility and thermogravimetric data were collected by using Sherwood MK-1 and SII 6300 TG/DTA, respectively. Molar conductivity measurements of the complexes were measured with a Hanna EC 215 conductivity meter by using 0.01 M KCl water solution as a calibrant.

4. 4. Enzyme assay

The activity of AChE was determined by the spectrophotometric method using acetylthiocholine iodide (ATC) as the substrate.⁴¹ The reaction mixture, in a final volume of 3 ml contained 60 μL of 75.0 mM ATC, 60 μL of 10.0 mM 5,5'-dithiobis(2-nitrobenzoic acid), 2.780 mL of 0.1 M potassium phosphate buffer, pH 8.0 and 100 μL of enzyme solution. The enzymatic reaction was initiated by adding the enzyme solution to the sample cuvette. Absorbance was read after 10 min incubation at 37 °C at 412 nm. Each activity value was taken from an average of 3–5 measurements. The inhibition effect was investigated by adding different volumes of 1 mM stock inhibitor solutions to the reaction mixtures which is here the buffer volume was reduced by the volume of inhibitor solution added. One unit of AChE (EU) was defined as the amount which catalyzed the hydrolysis of 1.0 μM of ATC per minute at room temperature, which was calculated based on an extinction coefficient of 13.6 $\text{mM}^{-1} \text{cm}^{-1}$.^{42,43}

The inhibition studies were performed with tacrine and edrophonium chloride, known specific inhibitors of acetylcholinesterase, and the synthesized complexes at pH 8.0 in the presence of ATC substrate. The inhibitory concentration (IC_{50}), which inhibits the AChE activity by 50%, was determined by using the % inhibition graph drawn against the inhibitory concentration. Inhibitors and their concentration ranges were as follows: tacrine 0.1–20.0 μM , edrophonium chloride 0.1–4.0 μM , and the complexes 2.0–30.0 μM . Each inhibitor was used in at least six concentrations.⁴⁴

4. 5. Theoretical Methodology

Quantum chemical calculations were performed to provide information about molecular geometry, electronic structure, molecular and spectroscopic properties. Fully optimized structural parameters of the ligands (H_2L and bipy) and their metal (Mn(II), Ni(II), Cu(II), Zn(II)) complexes were calculated at the DFT level (B3LYP) with basis sets 6-311++ G(d,p) for nonmetal atoms, LANL2DZ and the effective core potential (ECP) for metal atoms. Since the CAM-B3LYP method gives a better definition of the excited state transitions compared to the B3LYP function, the electronic excitations were calculated using TD-CAM-B3LYP methods and 6-311++G(2d,2p) basis set for nonmetal atoms and LANL2DZ with the effective core potential (ECP)

for metal atoms combined with a conductor-like polarizable continuum model (CPCM) in the implicit solvent of DMSO.⁴⁵ All calculations were done using the Gaussian 09 platform.⁴⁶ The optimized geometries and frontier molecular orbital (FMO) densities were visualized using the Gauss View 5 software. GAUSSSUM 3.0⁴⁷ to interpret the UV-Vis bands and analyze fractional contributions, and the VED-A4X⁴⁸ for analysis of elementary vibration modes were used.

4. 6. Synthesis of the Complexes- General Procedure

Firstly, ethanolic solution of NaOH was added to the solution of the ligand, H_2L (1 mmol) in 15 mL ethyl alcohol to neutralize. To this solution was added the solution of metal(II) perchlorate ($\text{Mn}(\text{ClO}_4)_2 \cdot 6\text{H}_2\text{O}$, $\text{Ni}(\text{ClO}_4)_2 \cdot 6\text{H}_2\text{O}$, $\text{Cu}(\text{ClO}_4)_2 \cdot 6\text{H}_2\text{O}$ or $\text{Zn}(\text{ClO}_4)_2 \cdot 6\text{H}_2\text{O}$) (1 mmol) in 10 mL ethyl alcohol. 2,2'-bipyridine (2.0 mmol for **1** and **2**; 1.0 mmol for **3-5**) in 10 mL ethyl alcohol was added to the solution, after the solution was stirred for 30 min at room temperature. The mixture was stirred for six hours at room temperature and then allowed to stand for two days at room temperature. Solid precipitate was filtered and washed with water and ethyl alcohol, respectively. Finally, the resulting solid powders were filtered, recrystallized from a hot DMSO- H_2O mixture and dried in vacuo over CaCl_2 . Single crystals couldn't be obtained for X-ray diffraction studies though our great efforts.

$[\text{Mn}(\text{HL})(\text{bipy})_2](\text{ClO}_4)_2$ (**1**)

Yield 0.25 g (35%). mp 290–296 °C (dec.). Color: Brownish khaki. FT-IR (cm^{-1}): 3100–3050 $\nu(\text{C-H})$; 1623, 1595 $\nu(\text{C=N})$; 1519, 1468, 1439 $\nu(\text{-C=C-})$; 1397 $\nu(\text{N=N})$; 1300 $\nu(\text{C-O})$; 1141, 1107 $\nu_3(\text{ClO}_4^-)$; 922 $\nu_1(\text{ClO}_4^-)$; 762 (bipy). UV-Vis. λ_{max} , nm (ϵ , $\text{M}^{-1} \text{cm}^{-1}$) in DMF: 291 (13880); 398 (8900); 461 (7300). Molar conductivity ($\Omega^{-1} \text{cm}^2 \text{mol}^{-1}$) 60. μ_{eff} B.M. (298 K): 5.80. MALDI-TOF MS (m/z): Calc. for $\text{C}_{33}\text{H}_{26}\text{ClN}_7\text{O}_6\text{Mn}$: 707.0; Found: 607.9 $[\text{M}-\text{ClO}_4]^+$. Anal. Calc.: C, 56.06; H, 3.71; N, 13.87. Found: C, 56.27; H, 3.62; N, 13.81.

$[\text{Ni}(\text{HL})(\text{bipy})_2](\text{ClO}_4)_2$ (**2**)

Yield 0.39 g (55%). mp 252–259 °C (dec.). Color: Greenish yellow. FT-IR (cm^{-1}): 3416 $\nu(\text{OH})$; 1644, 1602 $\nu(\text{C=N})$; 1575, 1495, 1472, 1440 $\nu(\text{-C=C-})$; 1409 $\nu(\text{N=N})$; 1314 $\nu(\text{C-O})$; 1082, 1071 $\nu_3(\text{ClO}_4^-)$; 945 $\nu_1(\text{ClO}_4^-)$; 763 (bipy). UV-Vis. λ_{max} , nm (ϵ , $\text{M}^{-1} \text{cm}^{-1}$) in DMF: 290 (16420); 433 (5740). Molar conductivity ($\Omega^{-1} \text{cm}^2 \text{mol}^{-1}$) 61. μ_{eff} B.M. (298 K): 2.60. MALDI-TOF MS (m/z): Calc. for $\text{C}_{33}\text{H}_{26}\text{ClN}_7\text{O}_6\text{Ni}$: 710.7; Found: 592.7 $[\text{M}-(\text{ClO}_4+\text{H}_2\text{O})]^+$. Anal. Calc.: C, 55.77; H, 3.69; N, 13.79. Found: C, 55.54; H, 3.52; N, 13.88.

$[\text{Ni}(\text{HL})(\text{bipy})(\text{ClO}_4)]_2$ (**3**)

Yield 0.24 g (43%). mp 248–257 °C (dec.). Color: Khaki. FT-IR (cm^{-1}): 3408 $\nu(\text{OH})$; 1644, 1606 $\nu(\text{C=N})$;

1548, 1476, 1440 $\nu(\text{C}=\text{C})$; 1409 $\nu(\text{N}=\text{N})$; 1310 $\nu(\text{C}-\text{O})$; 1157, 1115, 1085, 1071 $\nu_1, \nu_4(\text{OCLO}_3^-)$; 933 $\nu_2(\text{OCLO}_3^-)$; 763 (bipy). UV-Vis. λ_{max} , nm (ϵ , $\text{M}^{-1} \text{cm}^{-1}$) in DMF: 362 (15080); 429 (22350). Molar conductivity ($\Omega^{-1} \text{cm}^2 \text{mol}^{-1}$) 82. μ_{eff} B.M. (298 K): 1.81. MALDI-TOF MS (m/z): Calc. for $\text{C}_{23}\text{H}_{18}\text{ClN}_5\text{O}_6\text{Ni}$: 554.6; Found: 453.6 $[\text{M}-\text{ClO}_4]^+$. Anal. Calc.: C, 49.81; H, 3.27; N, 12.63. Found: C, 50.02; H, 3.33; N, 12.47.

$[\text{Cu}(\text{HL})(\text{bipy})(\text{ClO}_4)]$, (4)

Yield 0.26 g (46%). mp 209–215 °C (dec.). Color: Brown. FT-IR (cm^{-1}): 3440 $\nu(\text{OH})$; 1645, 1602 $\nu(\text{C}=\text{N})$; 1541, 1476, 1437 $\nu(\text{C}=\text{C})$; 1406 $\nu(\text{N}=\text{N})$; 1313 $\nu(\text{C}-\text{O})$; 1158, 1113, 1071 $\nu_1, \nu_4(\text{OCLO}_3^-)$; 924 $\nu_2(\text{OCLO}_3^-)$; 764 (bipy). UV-Vis. λ_{max} , nm (ϵ , $\text{M}^{-1} \text{cm}^{-1}$) in DMF: 290 (19760); 367 (39130); 459 (32540). Molar conductivity ($\Omega^{-1} \text{cm}^2 \text{mol}^{-1}$) 5. μ_{eff} B.M. (298 K): 2.1. MALDI-TOF MS (m/z): Calc. for $\text{C}_{23}\text{H}_{18}\text{ClN}_5\text{O}_6\text{Cu}$: 559.4; Found: 459.7 $[\text{M}-\text{ClO}_4]^+$. Anal. Calc.: C, 49.38; H, 3.24; N, 12.52. Found: C, 49.63.74; H, 3.39 N, 12.43.

$[\text{Zn}(\text{HL})(\text{bipy})(\text{ClO}_4)]$, (5)

Yield 0.16 g (29%). mp 281–289 °C (dec.). Color: Light orange. FT-IR (cm^{-1}): 3190 $\nu(\text{OH})$; 1603, 1544 $\nu(\text{C}=\text{N})$; 1477, 1441 $\nu(\text{C}=\text{C})$; 1405 $\nu(\text{N}=\text{N})$; 1287 $\nu(\text{C}-\text{O})$; 1145, 1111, 1070 $\nu_1, \nu_4(\text{OCLO}_3^-)$; 920 $\nu_2(\text{OCLO}_3^-)$; 763 (bipy). UV-Vis. λ_{max} , nm (ϵ , $\text{M}^{-1} \text{cm}^{-1}$) in DMF: 288 (22000); 352 (36270). ^1H NMR δ (400 MHz, $\text{DMSO}-d_6$): 11.15 bs. (1H, OH), 8.68 s. (1H, HC=N), 8.44 s. (2H, Ar), 8.07 s. (1H, Ar), 7.95 s. (2H, Ar), 7.77 d. (4H, Ar, J=8.0 Hz), 7.52 dd. (4H, Ar, J=8.0 Hz), 7.44 t. (2H, Ar, J=8.0 Hz), 6.87 s. (1H, Ar). Molar conductivity ($\Omega^{-1} \text{cm}^2 \text{mol}^{-1}$) 4. μ_{eff} B.M. (298 K): dia. MALDI-TOF MS (m/z): Calc. for $\text{C}_{23}\text{H}_{18}\text{ClN}_5\text{O}_6\text{Zn}$: 561.3; Found: 461.3 $[\text{M}-\text{ClO}_4]^+$. Anal. Calc.: C, 49.22; H, 3.23; N, 12.48. Found C, 49.08; H, 3.32; N, 12.44.

Declaration of Competing Interest

The authors declare that they have no known competing financial interests or personal relationships that could have appeared to influence the work reported in this paper.

Acknowledgments

Part of this work was financially supported by the Research Fund of Recep Tayyip Erdogan University (Project ID:1184). The numerical calculations reported in this paper were performed at TUBITAK ULAKBIM, High Performance, and Grid Computing Center (TRUBA Resources).

5. References

1. K. Serbest, T. Dural, M. Emirik, A. Zengin, Ö. Faiz, *J. Mol. Struct.* **2020**, 1229, 129579. DOI:10.1016/j.molstruc.2020.129579
2. M. Sarigul, P. Deveci, M. Kose, U. Arslan, H. Türk Dagi, M. Kurtoglu, *J. Mol. Struct.* **2015**, 1096, 64–73. DOI:10.1016/j.molstruc.2015.04.043
3. M. R. Lutfur, G. Hegde, S. Kumar, C. Tschierske, V. G. Chigrinov, *Opt. Mater. (Amst)*. **2009**, 32, 176–183. DOI:10.1016/j.optmat.2009.07.006
4. W. Zafar, S. H. Sumrra, & Z. H. Chohan, *Eur. J. Med. Chem.* **2021**, 222, 113602. DOI:10.1016/j.ejmech.2021.113602
5. S. Yasmeen, S. H. Sumrra, M. S. Akram, & Z. H. Chohan, *J. Enzyme Inhib. Med. Chem.* **2017**, 32, 106–112. DOI:10.1080/14756366.2016.1238363
6. S. Rani, S. H. Sumrra, & Z. H. Chohan, *Russ. J. Gen. Chem.* **2017**, 87, 1834–1842. DOI:10.1134/S107036321708031X
7. S. H. Sumrra, M. Hanif, Z. H. Chohan et al. *J. Enzyme Inhib. Med. Chem.* **2016**, 31, 590–598. DOI:10.3109/14756366.2015.1050011
8. S. H. Sumrra, U. Habiba, W. Zafar, M. Imran, & Z. H. Chohan, *J. Coord. Chem.* **2020**, 73, 2838–2877. DOI:10.1080/00958972.2020.1839751
9. M. Çol Ayyaz, İ. Turan, B. Dural, S. Demir, K. Karaoğlu, Y. Aliyazicioğlu, K. Serbest, *TURKISH J. Chem.* **2017**, 41, 728–747. DOI:10.3906/kim-1612-53
10. M. Ikram, Saeed-Ur-Rehman, S. Rehman, R.J. Baker, C. Schulzke, *Inorganica Chim. Acta* **2012**, 390, 210–216. DOI:10.1016/j.ica.2012.04.036
11. K. Bhagat, J. V. Singh, A. Sharma, A. Kaur, N. Kumar, H.K. Gulati, A. Singh, H. Singh, P. M. S. Bedi, *J. Mol. Struct.* **2021**, 1245, 131085. DOI:10.1016/j.molstruc.2021.131085
12. I. M. Dias, H. C. S. Junior, S. C. Costa, C. M. Cardoso, A. G. B. Cruz, C. E. R. Santos, D. R. S. Candela, S. Soriano, M. M. Marques, G. B. Ferreira, G. P. Guedes, *J. Mol. Struct.* **2020**, 1205, 127564. DOI:10.1016/j.molstruc.2019.127564
13. A. L. F. Sarria, A. F. L. Vilela, B. M. Fruger, J. B. Fernandes, R. M. Carlos, M. F. das G. F. da Silva, Q. B. Cass, C. L. Cardoso, *J. Inorg. Biochem.* **2016**, 164, 141–149. DOI:10.1016/j.jinorgbio.2016.09.010
14. S.-C. Tsaur, Some Fulgoroids (Insecta: Hemiptera) Collected on Turtle Island, Taiwan. *Zool. Stud.* **2005**, 44, 1–4.
15. T. Gokturk, A. Mihli, *Ann. Agrar. Sci.* **2016**, 14, 311–314. DOI:10.1016/j.aasci.2016.09.007
16. T. Göktürk, *Artvin Çoruh Üniversitesi Orman Fakültesi Derg.* **2015**, 16, 89–93. DOI:10.17474/acuofd.44749
17. J. Nast, *Palaearctic Auchenorrhyncha (Homoptera) an Annotated Checklist*. (Polish Scientific Publishers, Warszawa, 1972).
18. V. M. Gnezdilov, *Entomol. Rev.* **2009**, 89, 1082–1086. https://doi./10.1134/S0013873809090097
19. E. Demir, Riciania Germar, 1818 species of western palaearctic region (Hemiptera: fulgoromorpha: Ricaniidae). *Munis Entomol. Zool.* **2009**, 4, pp. 271–275.
20. J. M. Urban, J. R. Cryan, *Mol. Phylogenet. Evol.* **2007**, 42, 556–572. DOI:10.1016/j.ympev.2006.08.009
21. D. Fournier, A. Mutero, *Comp. Biochem. Physiol. Part C Pharmacol. Toxicol. Endocrinol.* **1994**, 108, 19–31. DOI:10.1016/1367-8280(94)90084-1
22. F. Li, Z. Han, *Arch. Insect Biochem. Physiol.* **2002**, 51, 37–45. DOI:10.1002/arch.10048

23. S. Keane, M. Ryan, *Insect Biochem. Mol. Biol.* **1999**, *29*, 1097–1104. DOI:10.1016/S0965-1748(99)00088-0
24. S. H. Sumrra, F. Mushtaq, F. Ahmad, R. Hussain, W. Zafar, M. Imran, M. N. Zafar, *Chem. Pap.* **2022**, *76*, 3705–3727. DOI:10.1007/s11696-022-02123-1
25. S. H. Sumrra, W. Zafar, H. Javed, M. Zafar, M. Z. Hussein, M. Imran, M. A. Nadeem, *BioMetals* **2021**, *34*, 1329–1351. DOI:10.1007/s10534-021-00345-6
26. S. H. Sumrra, Z. Arshad, W. Zafar, *et al. R. Soc. Open Sci.* **2021**, *8*, 210910. DOI:10.1098/rsos.210910
27. A. W. Addison, T. N. Rao, J. Reedijk, J. van Rijn, G. C. Verschoor, *J. Chem. Soc., Dalton Trans.* **1984**, 1349–1356. DOI:10.1039/DT9840001349
28. M. A. Said, A. Al-unizi, M. Al-Mamary, S. Alzahrani, D. Lentz, *Inorganica Chim. Acta* **2020**, *505*, 119434. DOI:10.1098/rsos.210910
29. R. V. Sakthivel, P. Sankudevan, P. Vennila, G. Venkatesh, S. Kaya, G. Serdaroğlu, *J. Mol. Struct.* **2021**, 1233, 130097. DOI:10.1016/j.molstruc.2021.130097
30. N. E. H. Bensiradj, A. Dekhira, N. Zouaghi, O. Ouamerli, *Struct. Chem.* **2020**, *31*, 1493–1503. DOI:10.1007/s11224-020-01509-9
31. K. Serbest, A. Özen, Y. Ünver, M. Er, İ. Değirmencioglu, K. Sancak, *J. Mol. Struct.* **2009**, 922, 1–10. DOI:10.1016/j.molstruc.2009.02.001
32. S. H. Sumrra, W. Zafar, M. L. Asghar, F. Mushtaq, M. A. Raza, M. F. Nazar, M. A. Nadeem, M. Imran, S. Mumtaz, *J. Mol. Struct.* **2021**, 1238, 130382. DOI:10.1016/j.molstruc.2021.130382
33. N. M. N. Gowda, S. B. Naikar, G. K. N. Reddy, Perchlorate Ion Complexes. **1984**, in 255–299. DOI:10.1016/S0898-8838(08)60210-X
34. M. Ghosh, P. Biswas, U. Flörke, *Polyhedron* **2007**, *26*, 3750–3762. DOI:10.1016/j.poly.2007.04.014
35. B. J. Hathaway, A. E. Underhill, *J. Chem. Soc.* **1961**, 3091–3096. DOI:10.1039/jr9610003091
36. N. A. Vyas, S. S. Bhat, A. S. Kumbhar, U. B. Sonawane *et al. Eur. J. Med. Chem.* **2014**, *75*, 375–381. DOI:10.1016/j.ejmech.2014.01.052
37. A. M. Bondžić, T. D. Lazarević-Pašti, A. R. Leskovic *et al. Eur. J. Pharm. Sci.* **2020**, *151*, 105376. DOI:10.1016/j.ejps.2020.105376
38. M. Junaid, N. Islam, M. K., Hossain, M. O. Ullah, M. A. Halim, *PLoS One* **2019**, *14*, e0211935. DOI:10.1371/journal.pone.0211935
39. S. Piersanti, M. Reborra, G. Salerno, S. Anton, *Insects* **2020**, *11*, 886. DOI:10.3390/insects11120886
40. G.-M. Shen, X.-N. Wang, W. Dou, J.-J. Wang, *Pest Manag. Sci.* **2012**, *68*, 1553–1563. DOI:10.1002/ps.3340
41. V. S. Zanon, J. A. Lima, T. Cuya, F. R. S. Lima, A. C. C. da Fonseca, J. G. Gomez, R. R. Ribeiro, T. C. C. França, M. D. Vargas, *J. Inorg. Biochem.* **2019**, *191*, 183–193. DOI:10.1016/j.jinorgbio.2018.11.019
42. J. Y. Son, S. Shin, K. H. Choi, I. K. Park, *Int. J. Biochem. Cell Biol.* **2002**, *34*, 204–210. DOI:10.1016/S1357-2725(01)00082-6
43. G. L. Ellman, K. D. Courtney, V. Andres, R. M. Featherstone, *Biochem. Pharmacol.* **1961**, *7*, 88–95. DOI:10.1016/0006-2952(61)90145-9
44. M. A. Mohamed, S. Shaaan, A.-E.M. Ghazy, A. A. Ali, A. M. Abd-Elaziz, M. M. E. Ghanem, S. A. Abd-Elghany, *Int. J. Biol. Macromol.* **2020**, *147*, 1029–1040. DOI:10.1016/j.ijbiomac.2019.10.071
45. J. Tomasi, B. Mennucci, R. Cammi, *Chem. Rev.* **2005**, *105*, 2999–3094. DOI:10.1021/cr9904009
46. M. J. Frisch, G. W. Trucks, H. B. Schlegel, G. E. Scuseria, M. A. Robb, M. A., Cheeseman, J. R., Scalmani, *et al.* Gaussian 09, revision A.02. **2009**.
47. N. M. O'boyle, A. L. Tenderholt, K. M. Langner, *J. Comput. Chem.* **2008**, *29*, 839–845. DOI:10.1002/jcc.20823
48. M. H. Jamroz. Vibrational Energy Distribution Analysis: VEDA 4 Program, Warsaw. **2004**.

Povzetek

Sintetizirali smo nove enojdrne ternarne komplekse prehodnih kovin: [M(HL)(bipy)₂]ClO₄, (M: Mn(II) v spojini **1**, Ni(II) v **2**), [M(HL)(bipy) (ClO₄)], (M: Ni(II) v spojini **3**, Cu(II) v **4**, Zn(II) v **5**) in ligandoma 2-[(hidroksiimino)metil]-4-[-fenildiazenil]fenol, H₂L, in 2,2'-bipiridin. Strukture dobljenih spojin smo preučili z različnimi analitskimi in spektroskopskimi metodami, kot so elementna analiza, FTIR, UV-Vis, NMR, MALDI-TOF masna spektrometrija in termična analiza. Teoretske raziskave smo opravili z DFT metodo in uporabo B3LYP funkcije z naborom osnov 6-311++G (d, p)/LanLD2Z. Elektronske prehode v kompleksih smo nadalje karakterizirali z metodo TD-DFT/CAM-B3LYP. IR meritve in termična analiza potrjujejo predpostavljene strukture. Inhibicijsko delovanje kompleksov smo dokazali s preiskavo učinkov na acetilholinesterazo (AChE) ekstrahirano iz odraslih primerkov in ličink *Ricania simulans*. Med preiskovanimi kompleksi ima največjo aktivnost spojina **5** z najnižjo vrednostjo IC₅₀ (3.2±0.8 μM) za AChE odraslih osebkov in spojina **3** z najnižjo vrednostjo IC₅₀ (4.6±0.8 μM) za AChE ličink.



Except when otherwise noted, articles in this journal are published under the terms and conditions of the Creative Commons Attribution 4.0 International License